

# Low defect-mediated reverse-bias leakage in (0001) GaN via high-temperature molecular beam epitaxy

J. J. M. Law,<sup>1,a)</sup> E. T. Yu,<sup>1,b),c)</sup> G. Koblmüller,<sup>2</sup> F. Wu,<sup>2</sup> and J. S. Speck<sup>2</sup>

<sup>1</sup>Department of Electrical and Computer Engineering, University of California, San Diego, La Jolla, California 92093-0407, USA

<sup>2</sup>Materials Department, University of California, Santa Barbara, Santa Barbara, California 93106-5050, USA

(Received 23 November 2009; accepted 22 February 2010; published online 12 March 2010)

Conductive atomic force microscopy, scanning electron microscopy, and x-ray diffraction were used to determine the effects of Ga/N flux ratio on the conductivity of current leakage paths in GaN grown by molecular beam epitaxy. Our data reveal a band of fluxes near  $\text{Ga}/\text{N} \approx 1$  for which these pathways ceased to be observable. We conclude that changes in surface defects surrounding or impurities along screw-component threading dislocations are responsible for their conductive nature. These observations suggest a method for controlling the primary source of reverse-bias Schottky contact leakage in *n*-type GaN grown by molecular beam epitaxy. © 2010 American Institute of Physics. [doi:10.1063/1.3360227]

Disproportionate reverse-bias leakage current in *n*-type Schottky contacts to GaN grown by molecular beam epitaxy (MBE) is an acute problem for nitride based electronic devices.<sup>1,2</sup> Growth of GaN by MBE has typically occurred at low temperatures and under Ga-rich conditions to maintain good surface/interface morphology, which is in contrast to N-rich growth that minimizes reverse-bias leakage but leads to poor surface/interface morphology.<sup>3</sup> Progress has been made in MBE growth of (0001) GaN under N-rich conditions at temperatures above the thermal decomposition regime ( $>750$  °C).<sup>4</sup> These conditions yielded layer-by-layer growth, low surface roughness [ $<1$  nm root mean square (rms) roughness], and high electron mobilities (in excess of 1100 cm<sup>2</sup>/V s for light doping at 300 K).<sup>5</sup>

We have used conductive atomic force microscopy (CAFM) to examine the effects of Ga/N flux ratio for growth at temperatures  $>750$  °C on the local conduction properties of (0001) GaN. Analysis of CAFM images showed that for samples grown at these temperatures there exists a narrow band of fluxes near  $\text{Ga}/\text{N} \approx 1$  where no local reverse-bias leakage occurred at the detection limit of our instrument. Field-emission scanning electron microscopy (FE-SEM) and x-ray diffraction (XRD) revealed consistent densities of screw-component threading dislocations across the range of Ga/N flux ratios. The observation of consistent densities of mixed and screw dislocations and absence of local reverse-bias leakage in MBE GaN are in contrast with previous studies that suggested that the conductivity of dislocations was determined predominately by the dislocation type, with only pure screw dislocations exhibiting highly conductive behavior.<sup>3,6</sup>

In this study, plasma-assisted MBE was used to grow 0.6–0.8 μm of Si-doped (0001) GaN homoepitaxial layers. The growth substrates were semi-insulating GaN templates

grown by metal-organic chemical vapor deposition on sapphire commercially available from Lumilog with total dislocation densities of approximately  $5 \times 10^8$  cm<sup>-2</sup>. All GaN layers were grown between 780 and 790 °C at constant N flux of 5.0 nm/min with Ga fluxes of 3.8, 4.2, 4.5, 5.5, 6.5, 7, and 14 nm/min. Details of the growth procedures and conditions have been described elsewhere.<sup>4,5</sup> All samples having Ga flux larger than 5 nm/min were grown as one continuous layer with constant Si doping (low-to-mid  $10^{16}$  cm<sup>-3</sup>) on top of the templates. The samples grown at Ga fluxes of 3.8 and 4.2 nm/min had the following layer structure: 50 nm of *p*-type (Mg doped) GaN, 200 nm unintentionally doped (UID) GaN, and 650 nm of slightly Si-doped (mid  $10^{16}$  cm<sup>-3</sup>) GaN. The sample grown at a Ga flux of 4.5 nm/min had the following layer structure: 50 nm of UID GaN, 200 nm of highly Si-doped (mid  $10^{18}$  cm<sup>-3</sup>) GaN, and 550 nm of slightly Si-doped (mid  $10^{16}$  cm<sup>-3</sup>) GaN. Samples were sonicated in trichloroethylene, acetone, isopropanol, methanol, and deionized water for 2 min prior to metallization by electron beam evaporation of 33 nm Ti, 77 nm of Al, 33 nm of Ti, and 88 nm of Au. The samples were then annealed at 650 °C for 3 min in 5% H<sub>2</sub>/N<sub>2</sub> forming gas. CAFM images were obtained with a Veeco Multimode atomic force microscope (AFM) with Nanoscope IIIa controller under ambient environmental conditions (approximately 20 °C and 50% relative humidity). A conductive diamond coated tip, which was kept in constant contact with the surface, acted as a Schottky contact to our sample. A reverse-bias condition was established by the application of a positive bias to an Ohmic contact on the sample while the current through the tip was measured with a transimpedance amplifier. We specify the potential of the Schottky probe-tip contact relative to the Ohmic sample contact. The CAFM signal reveals nonuniformities in sample conductivity.<sup>6</sup> The specific features of interest in this work were localized, highly conductive current leakage paths thought to be associated with threading dislocations.<sup>7</sup>

AFM topographs show that none of the samples in this study exhibit spiral hillocks on their surfaces, which are typical on the surfaces of GaN grown by MBE at lower tempera-

<sup>a)</sup>Present address: Department of Electrical and Computer Engineering, University of California, Santa Barbara, Santa Barbara, CA 93106, USA.

<sup>b)</sup>Electronic mail: ety@ece.utexas.edu.

<sup>c)</sup>Present address: Microelectronics Research Center, Department of Electrical and Computer Engineering, The University of Texas at Austin, Austin, TX 78758, USA.

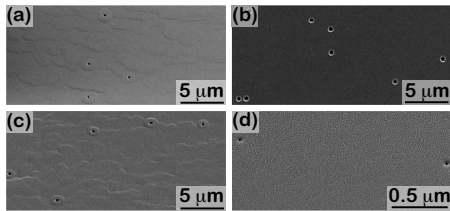


FIG. 1. FE-SEM images of sample grown at (a) 4.2 nm/min Ga-flux, (b) 7.0 nm/min Ga-flux, (c) 14.0 nm/min Ga-flux, and (d) substrate showing the surface terminations of open core screw-component threading dislocations.

tures under Ga-rich conditions;<sup>8</sup> however, all samples had smooth morphologies with nanometer-scale surface pit density matching the dislocation density of the substrates. The average pit densities, as measured by AFM, were  $6.1 \times 10^8$ ,  $6.5 \times 10^8$ ,  $6.16 \times 10^8$ ,  $6.6 \times 10^8$ ,  $6.4 \times 10^8$ ,  $6.2 \times 10^8$ , and  $5.5 \times 10^8 \text{ cm}^{-2}$  for samples with Ga fluxes of 3.8, 4.2, 4.5, 5.5, 6.5, 7.0, and 14.0 nm/min, respectively. XRD scans performed on samples grown with 4.2, 7, and 14 nm/min of Ga flux showed similar rocking curve widths for on-axis (0002)  $\omega$ -scan reflections with full-width at half-maximum (FWHM) of 393, 399, and 380 arc seconds, respectively. Since the FWHM of the rocking curves can be used to calculate the total *c*-component of all dislocations we conclude that the *c*-component of all dislocations across all samples were similar.<sup>9,10</sup> Figures 1(a)–1(d) show FE-SEM images of samples grown at 4.2, 7, and 14 nm/min Ga flux, and the substrate, likely illustrating the surface termination of open-core screw-component threading dislocations.<sup>11</sup> The density of these features was determined from larger images than those in Figs. 1(a)–1(d) to be  $\sim 6 \times 10^5$ ,  $2.5 \times 10^6$ ,  $7 \times 10^5$ , and  $1 \times 10^6 \text{ cm}^{-2}$  for the 4.2, 7, and 14 nm/min, and Lu-milog substrate samples. Based on the pit densities measured by AFM, the FWHM of (0002) rocking curves measured by XRD, and open core densities measured by FE-SEM, we conclude that the proportions of pure screw and mixed-component dislocations are consistent across all of the samples in this study.

Figure 2(a) shows an AFM topograph of a sample grown with a Ga flux of 4.5 nm/min. Figures 2(b)–2(d) show CAFM images obtained at dc biases of  $-14$ ,  $-18$ , and  $-22$  V corresponding to the area in Fig. 2(a). The wavy lines in Figs. 2(b)–2(d) are 60 Hz noise. The diagonal line in Fig. 2(c) is a systematic shift in the detected current which was most likely due to an external electrical noise source. Figure 2(b) shows several small, dark features that correspond to

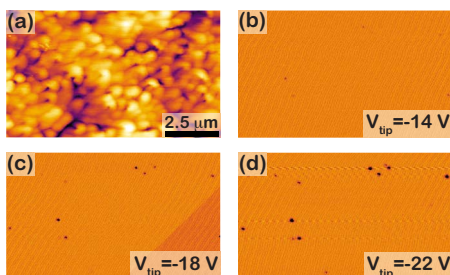


FIG. 2. (Color online) (a) AFM topograph and (b)–(d) CAFM images obtained at tip dc bias voltages of  $-14$ ,  $-18$ , and  $-22$  V for sample grown with 4.5 nm/min Ga flux. The conductive behavior for this sample is indicative of that for other N-rich samples. Wavy lines in (b)–(d) are 60 Hz noise. The scales correspond to range of 8 nm for topography and  $5 \times 10^{-11} \text{ A}$  for the current map.

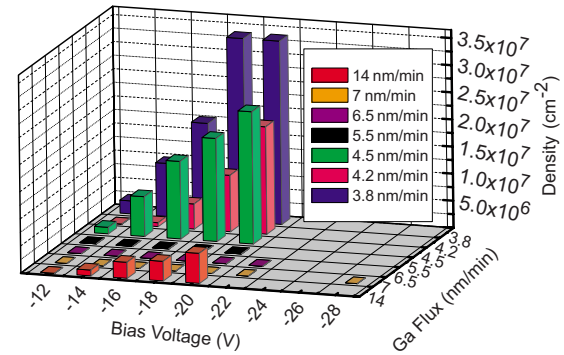


FIG. 3. (Color online) Conductive path densities vs bias voltage and Ga flux during growth.

localized reverse-bias leakage paths observable at  $-14$  V bias. In Fig. 2(c), the reverse-bias voltage magnitude was further increased and the density of observed conductive paths increased as well. This trend of increasing conductive path density as a function of increasing reverse-bias voltage magnitude continues in Fig. 2(d).

A more general analysis of the CAFM images for all samples suggests that at these elevated growth temperatures there is a narrow band of fluxes near  $\text{Ga}/\text{N} \approx 1$  for which there was no detectable localized reverse-bias leakage conduction. Figure 3 shows the conductive behavior of all the samples in this study as a function of reverse-bias voltage and Ga flux during growth. The sample with flux of 14.0 nm/min showed poor surface morphology—this sample was grown in the step-flow regime—with surface roughness  $\sim 3$  nm rms (measured over a  $5 \times 5 \mu\text{m}^2$  area) and reduced densities of leakage paths. Slightly Ga-rich samples with Ga fluxes of 7.0, 6.5, and 5.5 nm/min showed excellent morphologies with roughness less than 1 nm rms and no reverse-bias leakage at the highest level of sensitivity of our measurement technique ( $20 \text{ pA}$  and  $\sim 5 \times 10^5 \text{ cm}^{-2}$ ). The sample grown at 7.0 nm/min Ga flux showed no detectable leakage up to  $-28$  V. N-rich samples also showed excellent surface morphologies with roughness  $\sim 1.5$  nm rms, but, in contrast to their Ga-rich counterparts, showed increased reverse-bias leakage. In general, decreasing the Ga flux from 14.0 nm/min reduced the density of reverse-bias leakage paths until the crossover to N-rich growth at which point the conductive path density began to increase dramatically. The decreased density of leakage paths in the sample grown at 4.2 nm/min, as compared to the sample grown at 4.5 nm/min, was most likely due to the differences in underlying layer structure (as explained in the Experiment section above). Qualitatively, the trend of increasing reverse-bias leakage path density with decreasing Ga-flux (increasing N-flux) was the same for all N-rich samples.

Since the mechanism that allows for conduction from a dislocation into bulk material has not been definitively established, we cannot be certain that the inconsistent layer structure of the samples grown with Ga fluxes of 3.8, 4.2, and 4.5 nm/min samples does not influence our data. If the leakage current from the dislocation enters the bulk material within the first  $0.5$ – $0.8 \mu\text{m}$  of the top *n*-GaN layer, the current paths for all the samples should be similar and the lateral resistance in the sample should be substantially smaller than the resistance at the tip-sample junction. If the current from the dislocation enters the bulk material at greater depths, the

samples with Ga fluxes of 3.8 and 4.2 nm/min should exhibit low leakage by virtue of having an additional electrically insulating junction below the top *n*-GaN layer. However, these samples exhibit high leakage currents, roughly consistent with the sample grown at a Ga flux of 4.5 nm/min which has a highly conductive *n*<sup>+</sup>-GaN layer below the top *n*-GaN. Therefore, we conclude that the current is leaving the dislocation and entering the bulk within the first  $\sim$ 0.5–0.8  $\mu\text{m}$  of the top *n*-GaN layer, which is consistent across all of the samples in this study.

Consistent pit densities and FWHM of (0002)  $\omega$ -scans across the range of growth conditions suggest that the defect densities and compositions of all samples grown at high temperature are comparable. Therefore, it is unlikely that the absence of leakage paths in the slightly Ga-rich samples was a result of a reduction of the total number of defects or a change in the relative proportions of screw or screw-component threading dislocations. Because the maximum density of leakage paths ( $\sim$ mid  $10^7 \text{ cm}^{-2}$ ) in the N-rich samples was significantly larger than the expected pure screw threading dislocation density ( $\sim$ mid  $10^6 \text{ cm}^{-2}$ ), it is possible that both screw-component and pure screw threading dislocations are conducting,<sup>12</sup> indicating that it may not be solely the Burgers vector of the defect that dictates its conductive behavior. The Ga-rich, high-temperature growth conditions could have either modified the aggregation of impurities along the dislocations or surface defects surrounding the dislocations, with these impurities or defects being responsible for inducing local, reverse-bias leakage pathways. Prior studies of conductivity associated with threading dislocations have proposed that surface or near-surface defects can play an important role in controlling reverse-bias leakage currents associated with the presence of dislocations.<sup>13</sup> From a surface growth kinetics point of view, this could be influenced by differences in thermal dissociation behavior observed under different Ga/N flux ratios at the high growth temperatures employed in this study.<sup>14</sup>

CAFM, FE-SEM, and XRD were used to determine the effects of Ga/N flux ratio at elevated growth temperatures on the formation and conductive behavior of localized current leakage paths in GaN grown by MBE. Our data reveal a

narrow band of fluxes near  $\text{Ga}/\text{N} \approx 1$  for which local reverse-bias leakage paths ceased to be observable. The evolution of local reverse-bias leakage path density as a function of Ga flux at elevated growth temperature in conjunction with the consistent densities of screw and screw-component dislocations likely indicate that the conductive nature of these defects is determined by impurities along or surface defects near the dislocation. These observations are in contrast with previous studies that suggest it is not possible to simultaneously achieve smooth surfaces/interfaces and negligible local reverse-bias leakage,<sup>3</sup> and they could have substantial implications for the growth and expected performance of III-nitride based semiconductor devices.

The work at UCSD was supported in part by the NSF (ECS 0506902). The work at UCSB was supported by AFOSR (Don Silversmith and Kitt Reinhardt program managers) and ONR (Paul Maki program manager).

- <sup>1</sup>J. W. P. Hsu, M. J. Manfra, D. V. Lang, S. Richter, S. N. G. Chu, A. M. Sergent, R. N. Kleiman, L. N. Pfeiffer, and R. J. Molnar, *Appl. Phys. Lett.* **78**, 1685 (2001).
- <sup>2</sup>J. E. Northrup, *Appl. Phys. Lett.* **78**, 2288 (2001).
- <sup>3</sup>J. W. P. Hsu, M. J. Manfra, S. N. G. Chu, C. H. Chen, L. N. Pfeiffer, and R. J. Molnar, *Appl. Phys. Lett.* **78**, 3980 (2001).
- <sup>4</sup>G. Koblmüller, S. Fernández-Garrido, E. Calleja, and J. S. Speck, *Appl. Phys. Lett.* **91**, 161904 (2007).
- <sup>5</sup>G. Koblmüller, F. Wu, T. Mates, J. S. Speck, S. Fernández-Garrido, and E. Calleja, *Appl. Phys. Lett.* **91**, 221905 (2007).
- <sup>6</sup>J. W. P. Hsu, M. J. Manfra, R. J. Molnar, B. Heying, and J. S. Speck, *Appl. Phys. Lett.* **81**, 79 (2002).
- <sup>7</sup>E. J. Miller, D. M. Schaad, E. T. Yu, C. Poblenz, C. Elsass, and J. S. Speck, *J. Appl. Phys.* **91**, 9821 (2002).
- <sup>8</sup>B. Heying, E. J. Tarsa, C. R. Elsass, P. Fini, S. P. DenBaars, and J. S. Speck, *J. Appl. Phys.* **85**, 6470 (1999).
- <sup>9</sup>J. C. Zhang, D. G. Zhao, J. F. Wang, Y. T. Wang, J. Chen, J. P. Liu, and H. Yang, *J. Cryst. Growth* **268**, 24 (2004).
- <sup>10</sup>J. Q. Liu, J. F. Wang, Y. F. Liu, K. Huang, X. J. Hu, Y. M. Zhang, Y. Xu, K. Xu, and H. Yang, *J. Cryst. Growth* **311**, 3080 (2009).
- <sup>11</sup>Z. Liliental-Weber, Y. Chen, S. Ruvimov, and J. Washburn, *Phys. Rev. Lett.* **79**, 2835 (1997).
- <sup>12</sup>J. C. Moore, J. E. Ortiz, J. Xie, H. Morkoç, and A. A. Baski, *J. Phys.: Conf. Ser.* **61**, 90 (2007).
- <sup>13</sup>H. Zhang, E. J. Miller, and E. T. Yu, *J. Appl. Phys.* **99**, 023703 (2006).
- <sup>14</sup>S. Fernández-Garrido, G. Koblmüller, E. Calleja, and J. S. Speck, *J. Appl. Phys.* **104**, 033541 (2008).